

# Structure of the human glucagon class B G-protein-coupled receptor

Fai Yiu Siu<sup>1</sup>, Min He<sup>2</sup>, Chris de Graaf<sup>3</sup>, Gye Won Han<sup>1</sup>, Dehua Yang<sup>2</sup>, Zhiyun Zhang<sup>2</sup>, Caihong Zhou<sup>2</sup>, Qingping Xu<sup>4</sup>, Daniel Wacker<sup>1</sup>, Jeremiah S. Joseph<sup>1</sup>, Wei Liu<sup>1</sup>, Jesper Lau<sup>5</sup>, Vadim Cherezov<sup>1</sup>, Vsevolod Katritch<sup>1</sup>, Ming-Wei Wang<sup>2</sup> & Raymond C. Stevens<sup>1</sup>

**Binding of the glucagon peptide to the glucagon receptor (GCGR) triggers the release of glucose from the liver during fasting; thus GCGR plays an important role in glucose homeostasis. Here we report the crystal structure of the seven transmembrane helical domain of human GCGR at 3.4 Å resolution, complemented by extensive site-specific mutagenesis, and a hybrid model of glucagon bound to GCGR to understand the molecular recognition of the receptor for its native ligand. Beyond the shared seven transmembrane fold, the GCGR transmembrane domain deviates from class A G-protein-coupled receptors with a large ligand-binding pocket and the first transmembrane helix having a 'stalk' region that extends three alpha-helical turns above the plane of the membrane. The stalk positions the extracellular domain (~12 kilodaltons) relative to the membrane to form the glucagon-binding site that captures the peptide and facilitates the insertion of glucagon's amino terminus into the seven transmembrane domain.**

The glucagon receptor (GCGR) is one of the 15 members of the secretin-like (class B) family of G-protein-coupled receptors (GPCRs)<sup>1</sup> in humans. GCGR is activated by the 29 amino acid hormonal peptide glucagon (Supplementary Fig. 1a), and is a potential drug target for type 2 diabetes<sup>2</sup>. During fasting, the pancreas dispatches glucagon to activate GCGR in the liver causing the release of glucose into the blood<sup>2</sup>. Despite less than 15% protein sequence homology between class A (rhodopsin-like) and class B GPCRs, many of these receptors presumably share a seven transmembrane (7TM) helical domain and similar signal transduction mechanisms<sup>1</sup>. Although the structure–function understanding of the class A family of GPCRs has been greatly advanced during the last few years<sup>3</sup>, a detailed understanding of class B GPCRs has lagged due to the lack of a 7TM domain structure for these receptors.

Secretin-like GPCRs contain a globular N-terminal extracellular domain (ECD) defined by three conserved disulphide bonds<sup>4,5</sup> and a 7TM domain. They are activated by hormonal peptides that bind to both the ECD and the 7TM domain<sup>4</sup>. Structural details of soluble ECDs, including the ECD of GCGR<sup>6</sup>, and their role in the selective recognition of peptide hormones' carboxy termini have been revealed for several class B receptors<sup>5,7,8</sup>. Although models of class B 7TM domains and ligand binding have been proposed based on site-directed mutagenesis<sup>9–11</sup>, photo-crosslinking<sup>12–14</sup>, and structure-based virtual screening studies<sup>15</sup>, the accuracy of such modelling has been hampered by the low sequence homology between class A and class B GPCRs.

## Crystal structure of GCGR 7TM domain

The 7TM domain of human GCGR was fused to the thermally stabilized *E. coli* apocytocrome *b*<sub>562</sub>RIL (ref. 16) (referred to as BRIL) at residue 123, and the C terminus of GCGR was truncated at residue 432 (Supplementary Fig. 2). This crystallized GCGR construct with BRIL containing a truncated ECD ( $\Delta$ ECD) and C terminus ( $\Delta$ C) (BRIL–GCGR( $\Delta$ ECD/ $\Delta$ C)), Supplementary Fig. 3) has the same binding affinity for the antagonist ligand NNC0640 (Supplementary Fig. 1b) as the full-length wild-type GCGR (Supplementary Table 1), indicating

that the conformation of the 7TM domain of BRIL–GCGR( $\Delta$ ECD/ $\Delta$ C) is similar to wild-type GCGR. The structure of the BRIL–GCGR( $\Delta$ ECD/ $\Delta$ C) was determined at 3.4 Å resolution (Methods and Supplementary Table 2). Although GCGR was crystallized in the presence of NNC0640, convincing electron density for NNC0640 was not observed. As expected, GCGR adopts a 7TM fold (Fig. 1), with the BRIL fusion protein folded on top of the receptor and mediating most of the crystal contacts (Supplementary Fig. 4).

Despite the lack of protein sequence conservation, comparison of the GCGR 7TM structure with 15 known class A GPCR structures solved in inactive form shows that orientations and positions of helices in the 7TM bundles are conserved between the two classes (Fig. 1b, Supplementary Fig. 5). The 7TM helices of GCGR superimpose with those of the class A receptors with root mean squared deviation (r.m.s.d.) of C $\alpha$  backbone atoms in the 2.7–3.3 Å range, above the 2.2–3.0 Å range observed between major branches ( $\alpha$ ,  $\beta$ ,  $\gamma$  and  $\delta$ ) of class A GPCRs. The structural alignment of GCGR with rhodopsin shows an approximate spatial correspondence between residues in the 7TM helices of the two GPCR classes, but also reveals a number of gaps in transmembrane regions reflecting substantial structural deviations in transmembrane helices (Supplementary Fig. 6). The spatial correspondence between 7TM residues makes it possible to project the widely used class A Ballesteros–Weinstein numbering scheme<sup>17</sup> (used hereafter for class A as BW number in parentheses) for comparisons between GPCR classes (Supplementary Table 3). Analysis of sequence and structural features within class B GPCRs, however, is defined by the Wootten numbering scheme based on class B residue conservation<sup>18</sup> (used hereafter for class B receptors as superscript, Supplementary Table 3).

## Class B versus A GPCRs

The GCGR structure reveals a number of features in the 7TM domain that are distinct from known class A GPCRs. The N-terminal end of helix I in GCGR is longer than any known class A GPCR structures and extends three additional helical turns (approximately 16 Å) above

<sup>1</sup>Department of Integrative Structural and Computational Biology, The Scripps Research Institute, 10550 North Torrey Pines Road, La Jolla, California 92037, USA. <sup>2</sup>The National Center for Drug Screening and the CAS Key Laboratory of Receptor Research, Shanghai Institute of Materia Medica, Chinese Academy of Sciences (CAS), 189 Guo Shou Jing Road, Shanghai, 201203, China. <sup>3</sup>Division of Medicinal Chemistry, Faculty of Sciences, Amsterdam Institute for Molecules, Medicines and Systems (AIMMS), VU University of Amsterdam, De Boelelaan 1083, 1081 HV Amsterdam, The Netherlands. <sup>4</sup>The Joint Center for Structural Genomics, Stanford Synchrotron Radiation Lightsource, SLAC National Accelerator Laboratory, Menlo Park, California 94025, USA. <sup>5</sup>Protein & Peptide Chemistry, Novo Nordisk, Novo Nordisk Park, 2760 Malov, Denmark.

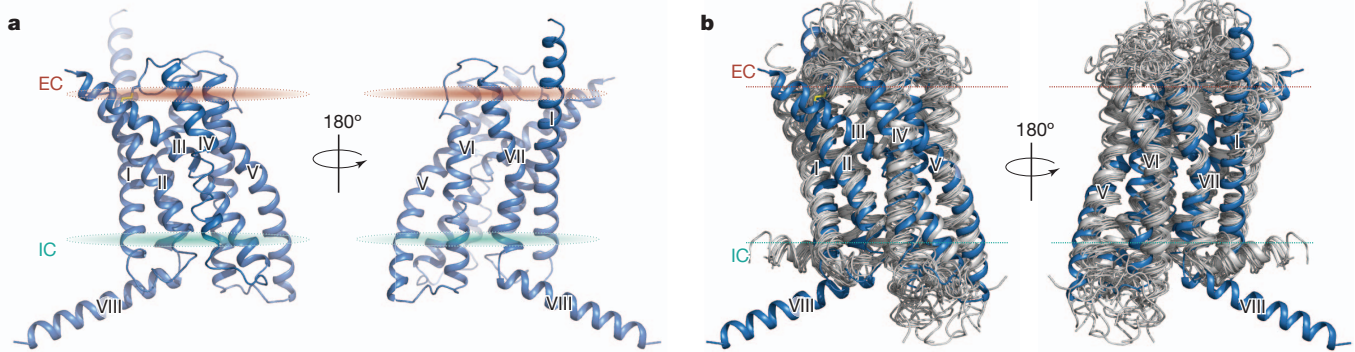


**Figure 1 | Structure of the 7TM domain of human GCGR and comparison to class A GPCR structures.** **a**, Cartoon depiction of the 7TM domain structure of GCGR. The two views are rotated 180° relative to each other. The disulphide bond between helix III and extracellular loop 2 (ECL2) is shown as yellow sticks. **b**, Side view of structural superimposition of 7TM domains of

the extracellular (EC) membrane boundary from Lys 136 to Gly 125 (Fig. 1). This region of GCGR, referred to as the stalk, may be involved in glucagon binding and helps to define the orientation of the ECD with respect to the 7TM domain. Extracellular loop 1 (ECL1) of GCGR is 16 residues long, as compared with 4–6 residues in most class A GPCRs. Although the ECL1 residues 201–215 are not resolved in the crystal structure, mutagenesis studies presented here and elsewhere<sup>19–21</sup> indicate that these residues are involved in interactions with peptide ligands. The distance between the EC tips of 7TM helices II and VI is the largest among GPCR structures, and the distance between the EC tips of helices III and VII is among the largest, except for kappa ( $\kappa$ -OR) and mu ( $\mu$ -OR) opioid receptors<sup>22,23</sup> (Supplementary Fig. 5). The positioning of the EC tips of these 7TM helices creates a wider and deeper cavity in the ligand-binding pocket of GCGR, which is larger than in any class A receptor structures (Fig. 2, Supplementary Table 4).

At the intracellular (IC) side, the distances between the helical tips of GCGR are within the same range as those in class A structures, except for an extensive inward shift of the IC tip of helix VII (Supplementary Fig. 5). Although the inward shift in the IC part of helix

GCGR (blue) and class A GPCRs (grey). Structures of class A GPCRs used (PDB): 1U19, 2RH1, 2YCW, 3RZE, 3PBL, 3UON, 4DAJ, 3EML, 3V2W, 3ODU, 4DJH, 4EA3, 4DKL, 4EJ4 and 3VW7. Extracellular (EC) and intracellular (IC) membrane boundaries (predicted by OMP server<sup>44</sup>) are shown as brown and cyan ovals (**a**) or dotted lines (**b**), respectively.

VII is a hallmark of class A receptor activation<sup>3</sup>, it is not yet clear what role the IC region of helix VII plays in GCGR. The receptor lacks a proline kink in helix VII, which is a part of the conserved NP (BW 7.50) xxY motif in class A GPCRs<sup>24</sup>; instead, helix VII of GCGR has a glycine residue (Gly 393<sup>7.50</sup>) that allows for a helical bend in this region. This glycine in helix VII of GCGR is part of the FQG<sup>7.50</sup>xxVxxxY<sup>7.57</sup>CF motif that is fully conserved in secretin-like class B receptors (Fig. 3a). This Gly 393<sup>7.50</sup> induced bend is stabilized by hydrophobic interactions with Phe 184<sup>2.57</sup> of helix II in GCGR (Fig. 3a).

The GCGR structure also includes an IC helix VIII comprising 20 residues at the C-terminal end of the receptor that tilts approximately 25° away from the membrane as compared with its consensus position in class A (Fig. 1). This tilt is probably a result of crystal packing interactions (Supplementary Fig. 4), but it should be noted that Glu 406 in helix VIII is fully conserved in secretin-like class B receptors, and forms two interhelical salt bridges with conserved residues Arg 173<sup>2.46</sup> and Arg 346<sup>6.37</sup> (Fig. 3b). Though the tilt of helix VIII may alter interactions in the region, conformational modelling with helix VIII parallel to the membrane suggests that the Glu 406 salt bridges are preserved in this

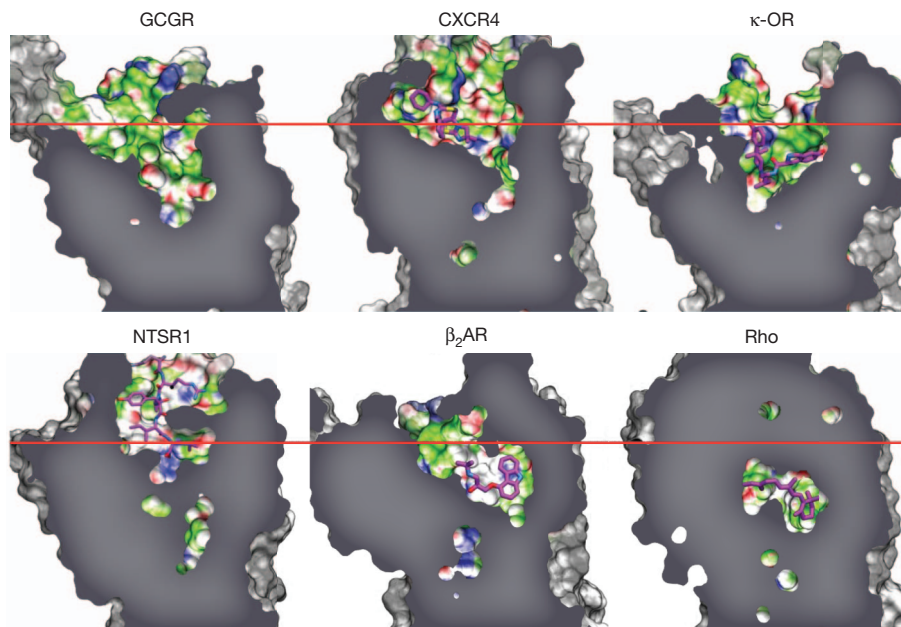


**Figure 2 | Comparison of the ligand-binding pocket of GCGR with class A GPCRs.** The binding cavity of GCGR is compared with the binding cavities of human chemokine receptor CXCR4 (PDB: 3ODU), human  $\kappa$ -opioid receptor ( $\kappa$ -OR) (PDB: 4DJH), rat neurotensin receptor (NTSR1) (PDB:

4GRV), human  $\beta_2$ -adrenergic receptor ( $\beta_2$ AR) (PDB: 2RH1) and bovine rhodopsin (Rho) (PDB: 1U19) (Supplementary Table 4). The approximate position of the EC membrane boundary is shown as a red line and bound ligands as magenta carbon atoms.

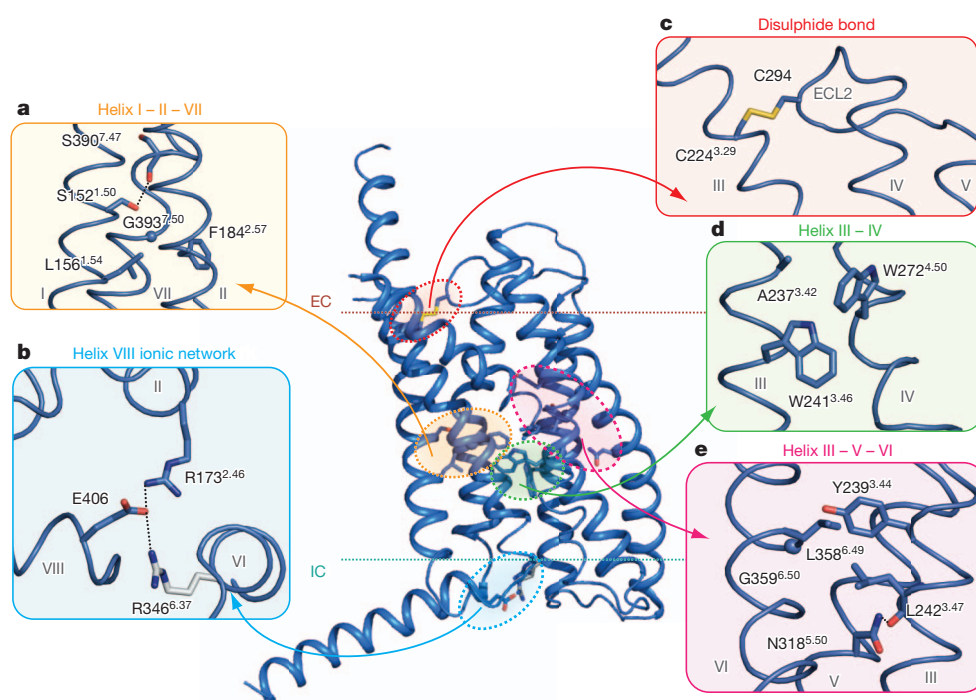


**Figure 3 | Structural features of class B GPCRs.** Comparison of GCGR and class A GPCR crystal structures indicates distinct and conserved features. **a, d, e,** The homologous GCGR residues involved in helix I–II, III–IV, and III–VI interface interactions as discussed for class A receptors by Venkatakrishnan *et al.*<sup>25</sup>, and class B GPCR specific residues that mediate helix I–VII, II–VII, and III–V interface interactions. **b,** GCGR residues Glu 406 of helix VIII, Arg 173<sup>2,46</sup>, and Arg 346<sup>6,37</sup> form a class B receptor specific ionic network. Arg 346<sup>6,37</sup> (grey) has a weak electron density. **c,** The disulphide bond between Cys 224<sup>3,29</sup> and Cys 294 of ECL2 in the GCGR structure is a conserved feature between classes A and B receptors. Hydrogen bond interactions and salt bridges are indicated by black dashed lines. Electron density maps for residues in this figure are shown in Supplementary Fig. 10. Comparison of class A Ballesteros–Weinstein and class B Wootten residue numbering is provided in Supplementary Table 3.

conformation and are likely to be a distinct feature of secretin-like class B receptors because there is no strong conservation among these residues in class A.

The GCGR 7TM structure also reveals several structural features that are conserved between class A and B receptors. One such feature is a disulphide bond between Cys 294 in ECL2 and Cys 224<sup>3,29</sup> (BW 3.25, Supplementary Fig. 6), which apparently stabilizes the receptor's 7TM fold (Fig. 3c). Another conserved feature of a common GPCR fold<sup>25</sup> involves similar regions of contacts between helices I–II, I–VII, III–IV and III–VI in class A and B GPCRs. The two GPCR classes, however, contain different patterns of conserved residues in these positions (Fig. 3, Supplementary Fig. 6). In class B GPCRs, the helix I–II interaction is stabilized by conserved hydrophobic residues Leu 156<sup>1,54</sup> and Phe 184<sup>2,57</sup>, class A GPCRs contain conserved polar residues Asn (BW 1.50) and Asp (BW 2.50) in this region<sup>25</sup>. At the helix I–VII interface, Ser 152<sup>1,50</sup> forms a hydrogen bond with the backbone of Ser 390<sup>7,47</sup> (Fig. 3a). Mutation of homologous glucagon-like peptide-1 receptor (GLP1R) residues Ser 155<sup>1,50</sup> and Ser 392<sup>7,47</sup> alters receptor signalling<sup>18</sup>. At the GCGR helix III–IV interface (Fig. 3d), the conserved residue Trp 272<sup>4,50</sup> interacts with Trp 241<sup>3,46</sup>, whereas in class A structures the Trp residue in helix IV (BW 4.50) interacts with the residue at BW position 3.38 in helix III (homologous GCGR residue Ala 237<sup>3,42</sup>) (refs 24, 25). The helix III–VI interface (Fig. 3e) in secretin-like class B GPCRs contains conserved hydrophobic residues Tyr 239<sup>3,44</sup> (or Phe<sup>3,44</sup>) and Leu 358<sup>6,49</sup> (or Phe<sup>6,49</sup>) which make similar hydrophobic interactions as structurally aligned Ile/Val/Leu (BW 3.40) and Phe (BW 6.44) residues present in most class A GPCRs<sup>25</sup> (Supplementary Fig. 6). This interface is further stabilized in class B GPCRs by close contact between the conserved Tyr 239<sup>3,44</sup> and Gly 359<sup>6,50</sup>. Another class B GPCR specific interhelical hydrogen bond is formed between the conserved Asn 318<sup>5,50</sup> and the backbone of Leu 242<sup>3,47</sup> at the helix III–V interface (Fig. 3e).

### Recognition between GCGR and glucagon

To better understand GCGR–glucagon interactions, we performed a comprehensive mutagenesis and glucagon-binding study of GCGR at 90 different residue positions (Fig. 4, Supplementary Table 5). A total

of 129 mutants were tested, and of these, 110 covering 85 different positions had expression levels greater than 30% of wild-type GCGR. Of them, 41 mutations covering 28 different positions in the GCGR 7TM domain had more than fourfold reduction in glucagon binding (IC<sub>50</sub> values) relative to wild-type GCGR. The results of these GCGR mutation studies were mapped onto the crystal structure of the GCGR 7TM domain (Fig. 5). Most of the residues that play an important role in glucagon binding face the main cavity in the 7TM core, and form a binding site that covers parts of ECL1, ECL2 and ECL3 and helices I, II, III, V, VI and VII, and extends deep into the 7TM cavity.

To investigate the recognition between glucagon and GCGR, we built a glucagon-bound GCGR structure model, based on the GCGR 7TM domain crystal structure, the GCGR ECD structure (Protein Data Bank (PDB) accession: 4ERS)<sup>6</sup>, the ECD structure of the GCGR homologue GLP1R bound to the GLP1 peptide (PDB: 3IOL)<sup>8</sup>, and the N-capped conformation of pituitary adenylate cyclase activating polypeptide (PACAP; PDB: 1GEA)<sup>26</sup> (Fig. 5a). The model further included several experimentally supported distance restraints between GCGR and glucagon based on photo-crosslinking studies between GLP1R and GLP1 (ref. 12).

The predicted binding mode of glucagon to the ECD of GCGR (Fig. 5b) is in line with our results (Fig. 4, Supplementary Table 5) and previously reported mutation studies on GCGR<sup>6,27</sup> and GLP1R<sup>8</sup>. Figure 5b shows how GCGR residues Asp 63, Tyr 65 and Lys 98 function in stabilizing the ECD as observed in the GCGR ECD crystal structure<sup>6</sup> and supported by mutagenesis studies<sup>6,27</sup> (Fig. 4, Supplementary Table 5). The Trp 36 side chain is an important hydrophobic interaction site for the C-terminal region of glucagon, similar to Trp 39 in the GLP1–GLP1R–ECD crystal structure<sup>8</sup>. The stalk, observed in helix I of the GCGR 7TM crystal structure, links the ECD and 7TM domain in the model (Figs 5a, b). The  $\alpha$ -helical conformation of the stalk is supported by intrahelical interactions in the crystal structure (Glu 133–Lys 136) and model (Glu 127–Gln 131 and Glu 129–Lys 132), and is likely to be further stabilized by interactions with the extended ECL1 and the  $\alpha$ -helical portion of glucagon. The potential function of the  $\alpha$ -helical stalk in glucagon binding is supported by a reduced glucagon affinity to the Ala 135 Pro mutant (Fig. 4d, Supplementary Table 5), which probably distorts the  $\alpha$ -helical

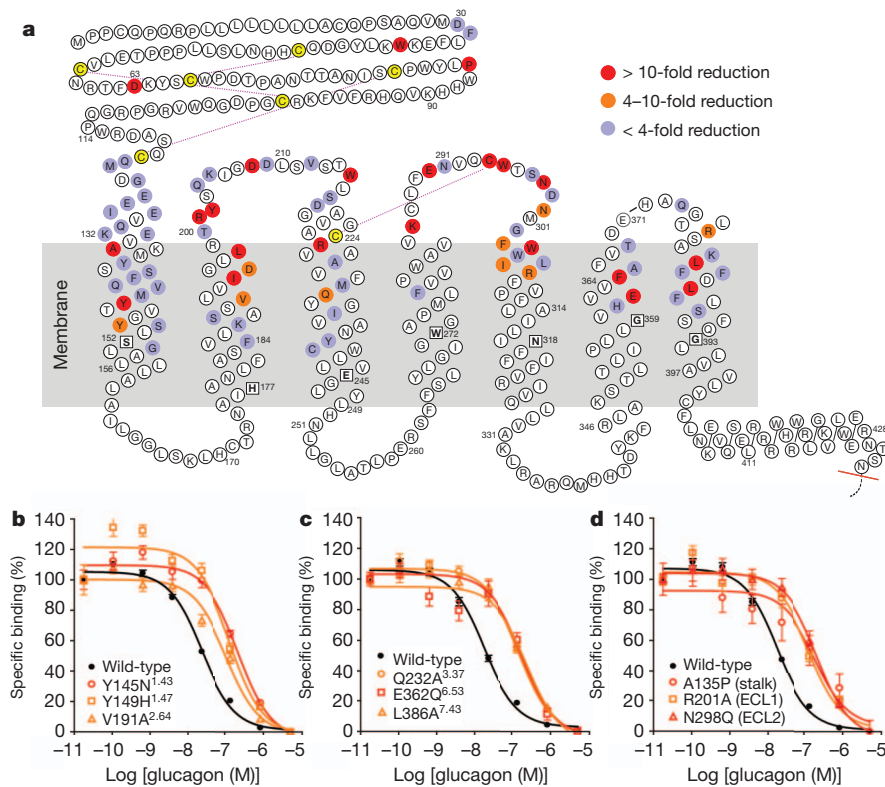


**Figure 4 | Effects of mutation studies in GPCR snake plot.** **a**, Mutated residues that show <4-fold (purple), 4–10-fold (orange), and >10-fold (red) changes of  $IC_{50}$  values for glucagon binding with receptor expression >30% of wild-type (Supplementary Table 5). Mutation studies to investigate peptide ligand binding have been previously reported for several class B GPCRs including GPCR<sup>6,19,21,27,31,32,34</sup>, GLP1R<sup>6,8,18,20,29,36</sup>, GIPR<sup>9,37</sup>, rSCTR<sup>11,30,35,38,43</sup> and VPAC1 (refs 39–41) (Supplementary Table 6). The most conserved residues in helices I to VII of class B GPCRs<sup>18</sup> are boxed and shown in bold. **b–d**, Representative binding curves of GPCR mutants with glucagon. Data are expressed as a percentage of specific <sup>125</sup>I-glucagon binding in the presence of 0.02 nM unlabelled peptide. Each point ( $\pm$  s.e.m.) represents the mean value of at least three independent experiments done in triplicate ( $IC_{50}$  are shown in Supplementary Table 5).

conformation of the stalk region. The stalk may also function as part of the binding site for the previously proposed middle hinge region of glucagon<sup>38</sup>. An  $\alpha$ -helical conformation in this region of GLP1R in complex with the GLP1 peptide was recently proposed based on cross-linking data between receptor and peptide residues<sup>12</sup>. In the GPCR–glucagon model, the corresponding pairs of residues, F6–Gln 142<sup>1,40</sup> and Y10–Tyr 138<sup>1,36</sup> (one letter amino acid abbreviation is used to designate glucagon residues), are located in close proximity and point towards each other, supporting a similar interaction mode as proposed in the GLP1R–GLP1 complex<sup>12</sup> (Fig. 5b). The 12 Å distance between L14–Trp 295<sup>ECL2</sup> in the GPCR–glucagon model exceeds the range of crosslinking distances in previous GLP1R–GLP1 models (8–9 Å)<sup>12</sup>, though this may reflect differences between GPCR and GLP1R ligand-binding modes.

There is no clear consensus on the binding site location of peptide ligands in the 7TM domain of class B GPCRs, which has been associated either with the ECL regions<sup>47</sup>, or with a pocket in the 7TM domain<sup>11,12,29</sup>. The GPCR–glucagon model illustrates a way to account for the extensive interactions of the peptide with ECLs, as well as residues deep in the 7TM domain (Fig. 5c, d). First, the GPCR crystal structure reveals that some of the binding site residues previously positioned at the top of 7TM helices or in ECLs<sup>30–32</sup> are in fact located deeper in the 7TM domain. Second, an extended flexible conformation of the first five residues allows glucagon to reach deep into the pocket. Our model of glucagon incorporates a hypothetical N-capping conformation<sup>33</sup> of the peptide helix in residues F6–T7–Y10, similar to the one observed in the receptor-bound PACAP<sup>26</sup>, though other conformations of this region are possible.

Most interactions predicted by the GPCR–glucagon binding model are supported by mutagenesis (Figs 4, 5c, d, Supplementary Table 5) and photo-crosslinking studies on GPCR<sup>6,19,21,27,31,32,34</sup> and other class B GPCRs<sup>8–13,20,29,30,35,36</sup>. In the 7TM domain, many residues predicted to interact with glucagon show dramatic effects on glucagon binding without reducing receptor expression (Fig. 4, Supplementary Table 5). Figure 5 shows how these mutations line the 7TM binding site in the GPCR–glucagon model and include residues that are located deep

in the pocket (Tyr 149<sup>1,47</sup>, Val 191<sup>2,64</sup>, Gln 232<sup>3,37</sup>, Glu 362<sup>6,53</sup> and Leu 386<sup>7,43</sup>). These results strongly support extension of the N terminus of glucagon deep into the GPCR pocket, a region that could be equally important for ligand binding as in class A GPCRs.

In the loop region, residues Arg 201, Tyr 202, Asp 208 and Trp 215 of GPCR either stabilize the ECL1 conformation and/or directly interact with glucagon (Fig. 5c, d). The GPCR–glucagon binding model further suggests that residues Trp 295 and Asn 298 directly interact with glucagon, as mutation of these ECL2 residues strongly affects ligand binding. Although mutations of Asp 218 (ref. 21), Cys 224<sup>3,29</sup> (refs 21, 27), Arg 225<sup>3,30</sup>, Lys 286<sup>4,64</sup>, Glu 290 and Cys 294 (Fig. 4, Supplementary Table 5) also affect ligand binding, these residues do not directly interact with glucagon in the model, but can play a role in stabilizing the loop conformation compatible with glucagon binding. For example, ECL2 and ECL1 are stabilized by a disulphide bridge between Cys 294 and Cys 224<sup>3,29</sup>, and potential salt bridges between Lys 286<sup>4,64</sup> and Glu 290, and between Asp 218 and Arg 225<sup>3,30</sup>, respectively. Similarly, Arg 378 is proposed to play a role in glucagon binding indirectly by stabilizing the ECL3 conformation, while Trp 304<sup>5,36</sup> stabilizes ECL2 at the interface between helices V and VI.

The GPCR–glucagon model presented in Fig. 5 is based on crystallographic evidence and is consistent with the results of extensive mutation binding studies (Fig. 4, Supplementary Table 5)<sup>6,19,21,27,31,32,34</sup>, and thus provides comprehensive insight into recognition between the native ligand and its receptor. The hypothetical model of the complex can offer a useful platform for the design of biochemical and biophysical experiments detailing the complex structure, as well as the design of stabilized constructs that may lead to solution of the full-length receptor–ligand complex.

### Related class B GPCRs

The GPCR–glucagon model can be informative for understanding common features that determine ligand recognition of other class B receptors. The GPCR mutation data (Fig. 4, Supplementary Table 5), and previous studies<sup>6,19,21,27,31,32,34</sup> are paralleled by mutagenesis of homologous residues in other class B GPCRs. Supplementary Table 6 shows

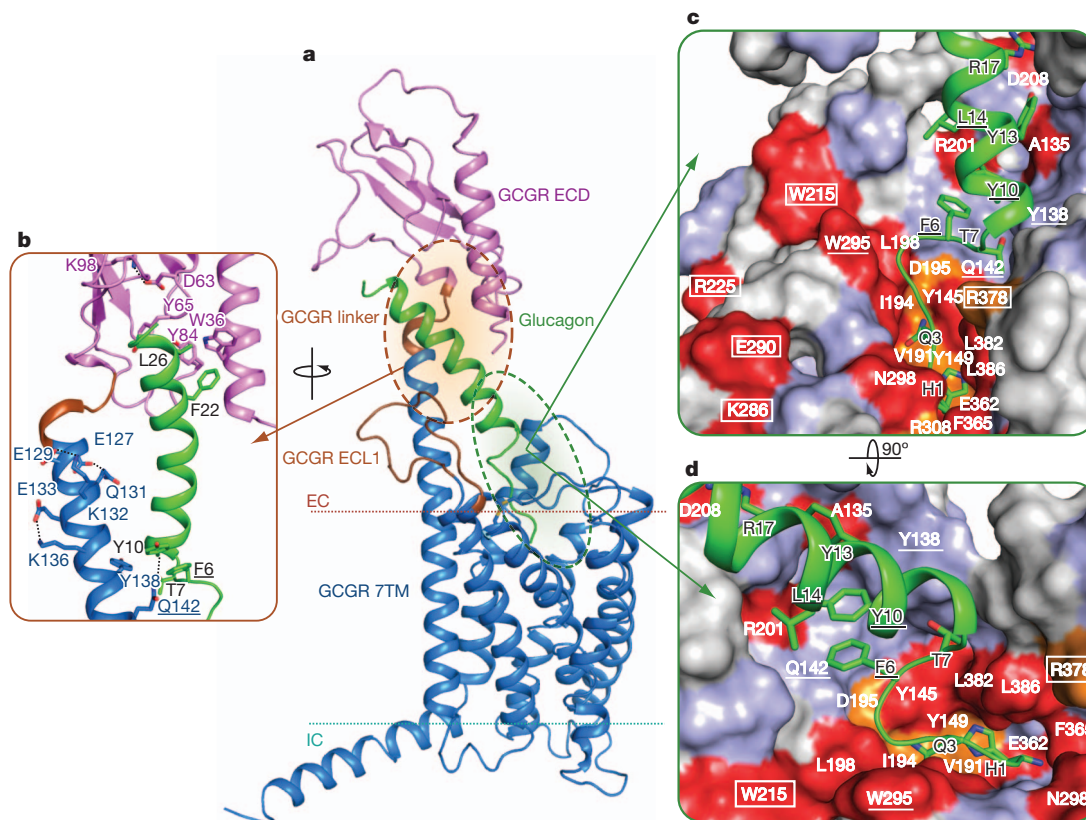


**Figure 5 | Model of GCGR bound to glucagon.** **a, b,** GCGR with the ECD (magenta) and 7TM domain (blue) bound to glucagon (green). Residues 122–126 and 199–218 (brown) are not defined in the GCGR ECD (GCGR-linker) (PDB: 4ERS) and 7TM domain (ECL1) crystal structures, respectively. The GCGR ECD structure and the interactions between GCGR ECD and glucagon resemble those in the GCGR ECD (PDB: 4ERS)<sup>6</sup> and GLP1–GLP1R-ECD complex (PDB: 3IOL)<sup>8</sup> structures, respectively. **c, d,** The effects of mutation

studies of individual GCGR residues on glucagon (green) binding mapped onto the GCGR binding surface using the colour coding presented in Fig. 4. Important glucagon residues are labelled black. GCGR residues proposed to be important in stabilizing extracellular loops are boxed. GCGR–glucagon residue pairs that are homologous to residue pairs identified in GLP1R–GLP1 crosslinking studies<sup>12</sup> are underlined.

an overview of 274 previously reported mutants of GCGR<sup>6,19,21,27,31,32,34</sup>, GLP1R<sup>8,18,20,29,36</sup>, glucose-dependent insulinotropic polypeptide receptor (also known as gastric inhibitory polypeptide receptor) (GIPR)<sup>9,37</sup>, rat secretin receptor (rSCTR)<sup>11,30,35,38,43</sup>, and vasoactive intestinal peptide and pituitary adenylate cyclase-activating polypeptide receptor 1 (VPAC1, also known as VIPR1) (refs 39–41). For example, mutations of other class B GPCRs in residues that align to GCGR residues Tyr 65<sup>ECD</sup> (ref. 8), Tyr 84<sup>ECD</sup> (ref. 8), Leu 85<sup>ECD</sup> (ref. 8), Tyr 145<sup>1,43</sup> (ref. 35), Tyr 149<sup>1,47</sup> (refs 29, 35), Lys 187<sup>2,60</sup> (refs 9, 18, 20, 29, 30, 39), Ile 194<sup>2,67</sup> (refs 9, 18, 20, 29, 30, 39), Asp 195<sup>2,68</sup> (refs 11, 20, 29, 30), Leu 198<sup>2,71</sup> (refs 11, 21), Arg 225<sup>3,30</sup> (ref. 20), Gln 232<sup>3,37</sup> (refs 9, 29), Lys 286<sup>4,64</sup> (ref. 36), Glu 290<sup>ECL2</sup> (ref. 36), Trp 295<sup>ECL2</sup> (refs 11, 36), Asn 298<sup>ECL2</sup> (refs 11, 36), Phe 365<sup>5,56</sup> (refs 9, 11) and Leu 386<sup>7,43</sup> (ref. 40) have been shown to affect peptide ligand binding and/or potency, supporting the GCGR–glucagon model in Fig. 5. The GCGR–glucagon model demonstrates that residues which have been identified to interact with the homologous residues Q3 of glucagon, D3 of secretin, and D3 of vasoactive intestinal peptide are located within the same vicinity in the 7TM domain of GCGR (Lys 187<sup>2,60</sup> and Ile 194<sup>2,67</sup>) (refs 31, 32), rSCTR (Tyr 128<sup>1,47</sup>, Arg 166<sup>2,60</sup>, Lys 173<sup>2,67</sup>, and Asp 174<sup>2,68</sup>) (refs 30, 35), and VPAC1 (Arg 188<sup>2,60</sup> and Lys 195<sup>2,67</sup>) (ref. 39), respectively (Supplementary Table 6).

The distinct structural features and larger binding pocket of the GCGR 7TM domain provide new insights into the molecular details of peptide ligand binding, and a more reliable structural template for the design of specific and potent small molecules for the treatment of type 2 diabetes. Moreover, the apparent overlap of class B GPCR binding sites suggests that, despite possible structural differences

between class B GPCRs, the GCGR crystal structure might offer new opportunities to construct structural models to describe interactions between peptide ligands and other class B GPCRs. This is particularly exciting for those receptors involved in glucose regulation, including GLP1R and GIPR.

## METHODS SUMMARY

BRIL–GCGR( $\Delta$ ECD/ $\Delta$ C) was expressed in *Spodoptera frugiperda* insect cells, solubilized with 1/0.1% (w/v) of *n*-dodecyl- $\beta$ -D-maltopyranoside and cholesteryl hemisuccinate for 2 h at 4 °C, and purified by immobilized metal ion affinity chromatography with 50–200  $\mu$ M of GCGR antagonist ligand NNC0640. Protein at 80 mg ml<sup>-1</sup> was mixed with monoolein and cholesterol in a ratio of 40%:54%:6% (w/w/w) to form lipidic cubic phase<sup>42</sup>, and crystallized in 100 mM MES pH 6.0, 140–200 mM Na/K tartrate tetrahydrate, 9–17% (v/v) PEG 400, 0.35–0.55% (v/v) Jeffamine M-600, pH 7.0, and 200  $\mu$ M NNC0640 at 20 °C. X-ray data were collected on the 23ID-D beamline (GM/CA CAT) at the Advanced Photon Source (Argonne, Illinois) using a 20- $\mu$ m minibeam at wavelength of 1.0330 Å (Supplementary Table 2). A single wavelength anomalous dispersion (SAD) data set was collected at 4 Å from a single crystal soaked with tantalum bromide (Ta<sub>6</sub>Br<sub>12</sub>; Supplementary Fig. 7). Phase information from the SAD data set confirmed the molecular replacement solution obtained from an auto script that used mixed models of all known class A GPCR structures as search models (Supplementary Fig. 8). Native diffraction data were collected from 14 crystals and anisotropically truncated before refinement in a\*, b\*, and c\* to 3.3, 3.4, and 3.3 Å, respectively. We report the final structure at 3.4 Å resolution, and data collection, processing, structure solution and refinement are described in the Methods.

The model of the GCGR–glucagon complex was constructed using the structures of the GCGR 7TM domain presented here, the GCGR ECD (PDB: 4ERS), the GLP1R–GLP1 complex (PDB: 3IOL), and the N-capped conformation of PACAP (PDB: 1GEA).

Binding studies were performed using transiently transfected CHO-K1 and HEK293T cells. Either whole cells or prepared membranes were used to measure binding affinity (IC<sub>50</sub>) of glucagon or NNC0640 using radiolabelled glucagon or NNC0640.

**Full Methods** and any associated references are available in the online version of the paper.

**Received 7 March; accepted 17 June 2013.**

**Published online 17 July 2013.**

- Lagerström, M. C. & Schiöth, H. B. Structural diversity of G protein-coupled receptors and significance for drug discovery. *Nature Rev. Drug Discov.* **7**, 339–357 (2008).
- Cho, Y. M., Merchant, C. E. & Kieffer, T. J. Targeting the glucagon receptor family for diabetes and obesity therapy. *Pharmacol. Ther.* **135**, 247–278 (2012).
- Katritch, V., Cherezov, V. & Stevens, R. C. Structure-function of the G protein-coupled receptor superfamily. *Annu. Rev. Pharmacol. Toxicol.* **53**, 531–556 (2013).
- Hoare, S. R. Mechanisms of peptide and nonpeptide ligand binding to class B G-protein-coupled receptors. *Drug Discov. Today* **10**, 417–427 (2005).
- Pal, K., Melcher, K. & Xu, H. E. Structure and mechanism for recognition of peptide hormones by Class B G-protein-coupled receptors. *Acta Pharmacol. Sin.* **33**, 300–311 (2012).
- Koth, C. M. et al. Molecular basis for negative regulation of the glucagon receptor. *Proc. Natl Acad. Sci. USA* **109**, 14393–14398 (2012).
- Parthier, C., Reedtz-Runge, S., Rudolph, R. & Stubbs, M. T. Passing the baton in class B GPCRs: peptide hormone activation via helix induction? *Trends Biochem. Sci.* **34**, 303–310 (2009).
- Underwood, C. R. et al. Crystal structure of glucagon-like peptide-1 in complex with the extracellular domain of the glucagon-like peptide-1 receptor. *J. Biol. Chem.* **285**, 723–730 (2010).
- Yaqub, T. et al. Identification of determinants of glucose-dependent insulinotropic polypeptide receptor that interact with N-terminal biologically active region of the natural ligand. *Mol. Pharmacol.* **77**, 547–558 (2010).
- Miller, L. J., Dong, M., Harikumar, K. G. & Gao, F. Structural basis of natural ligand binding and activation of the Class II G-protein-coupled secretin receptor. *Biochem. Soc. Trans.* **35**, 709–712 (2007).
- Dong, M. et al. Mapping spatial approximations between the amino terminus of secretin and each of the extracellular loops of its receptor using cysteine trapping. *FASEB J.* **26**, 5092–5105 (2012).
- Miller, L. J. et al. Refinement of glucagon-like peptide 1 docking to its intact receptor using mid-region photolabile probes and molecular modeling. *J. Biol. Chem.* **286**, 15895–15907 (2011).
- Dong, M. et al. Molecular basis of secretin docking to its intact receptor using multiple photolabile probes distributed throughout the pharmacophore. *J. Biol. Chem.* **286**, 23888–23899 (2011).
- Gensure, R. C., Shimizu, N., Tsang, J. & Gardella, T. J. Identification of a contact site for residue 19 of parathyroid hormone (PTH) and PTH-related protein analogs in transmembrane domain two of the type 1 PTH receptor. *Mol. Endocrinol.* **17**, 2647–2658 (2003).
- de Graaf, C., Rein, C., Piwnicka, D., Giordanetto, F. & Rognan, D. Structure-based discovery of allosteric modulators of two related class B G-protein-coupled receptors. *ChemMedChem* **6**, 2159–2169 (2011).
- Chun, E. et al. Fusion partner toolchest for the stabilization and crystallization of G protein-coupled receptors. *Structure* **20**, 967–976 (2012).
- Ballesteros, J. A. & Weinstein, I. In *Methods in Neurosciences* Vol. 25 (ed. Sealfon, S. C.) 366–428 (Academic Press, 1995).
- Wooten, D., Simms, J., Miller, L. J., Christopoulos, A. & Sexton, P. M. Polar transmembrane interactions drive formation of ligand-specific and signal pathway-biased family B G protein-coupled receptor conformations. *Proc. Natl Acad. Sci. USA* **110**, 5211–5216 (2013).
- Unson, C. G. et al. Roles of specific extracellular domains of the glucagon receptor in ligand binding and signaling. *Biochemistry* **41**, 11795–11803 (2002).
- Xiao, Q., Jeng, W. & Wheeler, M. B. Characterization of glucagon-like peptide-1 receptor-binding determinants. *J. Mol. Endocrinol.* **25**, 321–335 (2000).
- Roberts, D. J., Vertongen, P. & Waelbroeck, M. Analysis of the glucagon receptor first extracellular loop by the substituted cysteine accessibility method. *Peptides* **32**, 1593–1599 (2011).
- Wu, H. et al. Structure of the human  $\kappa$ -opioid receptor in complex with JDTic. *Nature* **485**, 327–332 (2012).
- Manglik, A. et al. Crystal structure of the  $\mu$ -opioid receptor bound to a morphinan antagonist. *Nature* **485**, 321–326 (2012).
- Fredriksson, R., Lagerström, M. C., Lundin, L. G. & Schiöth, H. B. The G-protein-coupled receptors in the human genome form five main families. Phylogenetic analysis, paralogon groups, and fingerprints. *Mol. Pharmacol.* **63**, 1256–1272 (2003).
- Venkatakrishnan, A. J. et al. Molecular signatures of G-protein-coupled receptors. *Nature* **494**, 185–194 (2013).
- Inooka, H. et al. Conformation of a peptide ligand bound to its G-protein coupled receptor. *Nature Struct. Biol.* **8**, 161–165 (2001).
- Prévost, M. et al. Mutational and cysteine scanning analysis of the glucagon receptor N-terminal domain. *J. Biol. Chem.* **285**, 30951–30958 (2010).
- Ahn, J. M., Medeiros, M., Trivedi, D. & Hruby, V. J. Development of potent truncated glucagon antagonists. *J. Med. Chem.* **44**, 1372–1379 (2001).
- Coopman, K. et al. Residues within the transmembrane domain of the glucagon-like peptide-1 receptor involved in ligand binding and receptor activation: modelling the ligand-bound receptor. *Mol. Endocrinol.* **25**, 1804–1818 (2011).
- Di Paolo, E. et al. Contribution of the second transmembrane helix of the secretin receptor to the positioning of secretin. *FEBS Lett.* **424**, 207–210 (1998).
- Perret, J. et al. Mutational analysis of the glucagon receptor: similarities with the vasoactive intestinal peptide (VIP)/pituitary adenylate cyclase-activating peptide (PACAP)/secretin receptors for recognition of the ligand's third residue. *Biochem. J.* **362**, 389–394 (2002).
- Runge, S. et al. Three distinct epitopes on the extracellular face of the glucagon receptor determine specificity for the glucagon amino terminus. *J. Biol. Chem.* **278**, 28005–28010 (2003).
- Neumann, J. M. et al. Class-B GPCR activation: is ligand helix-capping the key? *Trends Biochem. Sci.* **33**, 314–319 (2008).
- Cascieri, M. A. et al. Characterization of a novel, non-peptidyl antagonist of the human glucagon receptor. *J. Biol. Chem.* **274**, 8694–8697 (1999).
- Di Paolo, E. et al. Mutations of aromatic residues in the first transmembrane helix impair signalling by the secretin receptor. *Receptors Channels* **6**, 309–315 (1999).
- Koole, C. et al. Second extracellular loop of human glucagon-like peptide-1 receptor (GLP-1R) has a critical role in GLP-1 peptide binding and receptor activation. *J. Biol. Chem.* **287**, 3642–3658 (2012).
- Tseng, C. C. & Lin, L. A point mutation in the glucose-dependent insulinotropic peptide receptor confers constitutive activity. *Biochem. Biophys. Res. Commun.* **232**, 96–100 (1997).
- Ganguli, S. C. et al. Protean effects of a natural peptide agonist of the G protein-coupled secretin receptor demonstrated by receptor mutagenesis. *J. Pharmacol. Exp. Ther.* **286**, 593–598 (1998).
- Solano, R. M. et al. Two basic residues of the h-VPAC1 receptor second transmembrane helix are essential for ligand binding and signal transduction. *J. Biol. Chem.* **276**, 1084–1088 (2001).
- Ceraudo, E. et al. Spatial proximity between the VPAC1 receptor and the amino terminus of agonist and antagonist peptides reveals distinct sites of interaction. *FASEB J.* **26**, 2060–2071 (2012).
- Tan, Y. V., Couvineau, A. & Laburthe, M. Diffuse pharmacophoric domains of vasoactive intestinal peptide (VIP) and further insights into the interaction of VIP with the N-terminal ectodomain of human VPAC1 receptor by photoaffinity labeling with [Bpa6]-VIP. *J. Biol. Chem.* **279**, 38889–38894 (2004).
- Caffrey, M. & Cherezov, V. Crystallizing membrane proteins using lipidic mesophases. *Nature Protocols* **4**, 706–731 (2009).
- Di Paolo, E. et al. Role of charged amino acids conserved in the vasoactive intestinal polypeptide/secretin family of receptors on the secretin receptor functionality. *Peptides* **20**, 1187–1193 (1999).
- Lomize, M. A., Pogozheva, I. D., Joo, H., Mosberg, H. I. & Lomize, A. L. OPM database and PPM web server: resources for positioning of proteins in membranes. *Nucleic Acids Res.* **40**, D370–D376 (2012).

**Supplementary Information** is available in the online version of the paper.

**Acknowledgements** This work was supported by NIH Roadmap grant P50 GM073197 for technology development (V.C. and R.C.S.), and PSI:BiologY grant U54 GM094618 for biological studies and structure production (target GPCR-49) (V.K., V.C. and R.C.S.); PSI:BiologY grant U54 GM094586 for structure QC; The Ministry of Health grants 2012ZX09304-011 and 2013ZX09507002 (M.-W.W.), Shanghai Science and Technology Development Fund 11DZ2292200 (M.-W.W.); Novo Nordisk-Chinese Academy of Sciences Research Fund NNCAS-2011-7 (M.-W.W.); Thousand Talents Program in China (R.C.S. and M.-W.W.); NIH Postdoctoral Training Grant (NRSA) F32 DK088392 (F.Y.S.); The Netherlands Organization for Scientific Research (NWO) through a VENI grant (Grant 700.59.408 to C.d.G.); COST Action CM1207, GLISTEN (C.d.G.). We also thank V. Hruby and M. Cai for advice with the glucagon binding assay and general discussions; J. Velasquez for help with molecular biology; T. Trinh and M. Chu for help with baculovirus expression; K. Kadyshkevskaya for assistance with figure preparation; X. Q. Cai, J. Wang, Y. Feng, A. T. Dai, Y. Zhou, J. J. Deng, Y. B. Dai and J. W. Zhao for technical assistance in mutation studies; A. Walker for assistance with manuscript preparation; and J. Smith and R. Fischetti for assistance in development and use of the minibeam and beamtime at GM/CA-CAT beamline 23-ID at the Advanced Photon Source, which is supported by National Cancer Institute grant Y1-CO-1020 and National Institute of General Medical Sciences grant Y1-GM-1104.

**Author Contributions** F.Y.S. designed, expressed, characterized and screened constructs and ligands for crystallization. F.Y.S. purified and crystallized the receptor in LCP, optimized crystallization conditions, grew crystals, collected diffraction data and prepared the manuscript. G.W.H. and Q.X. solved and refined the structure, and prepared the manuscript. V.C. collected and processed diffraction data, and prepared the manuscript. M.H., D.Y., Z.Z. and C.Z. expressed the receptor, and performed the mutagenesis and ligand-binding assay. V.K. and C.d.G. designed and analysed the receptor mutagenesis studies, constructed the receptor-ligand model and prepared the manuscript. D.W. and J.S.J. collected and processed SAD data and determined an initial electron density map from experimental phases. W.L. and V.C. trained and assisted in LCP crystallization. J.L. provided ligands for GPCR and prepared the manuscript. R.C.S., F.Y.S., M.-W.W., V.K., V.C. and C.d.G. were responsible for the overall project strategy and management and wrote the manuscript.

**Author Information** The coordinates and the structure factors have been deposited in the Protein Data Bank under the accession code 4L6R. Reprints and permissions information is available at [www.nature.com/reprints](http://www.nature.com/reprints). The authors declare no competing financial interests. Readers are welcome to comment on the online version of the paper. Correspondence and requests for materials should be addressed to R.C.S. ([stevens@scripps.edu](mailto:stevens@scripps.edu)) or M.-W.W. ([wangmw@mail.shnc.ac.cn](mailto:wangmw@mail.shnc.ac.cn)).

## METHODS

**BRIL-GCGR( $\Delta$ ECD/ $\Delta$ C) construct design and S9 expression.** The human wild-type GCGR DNA was synthesized by DNA 2.0 and codon optimized for expression in *Spodoptera frugiperda* (Sf9) insect cells. The BRIL-GCGR( $\Delta$ ECD/ $\Delta$ C) fusion construct was made by deleting N-terminal residues 1–122, fusing the thermally stabilized apocytochrome *b*<sub>562</sub>RIL (M7W, H102I, R106L) (referred to as BRIL) from *E. coli* at residue 123 (ref. 16), and truncating the C terminus at residue 432 to create the final construct for crystallization (Supplementary Fig. 2). This chimaeric construct was obtained after screening 60 constructs of different BRIL junction and C-terminal truncation sites to generate crystals with diffraction data of the highest quality and resolution. The construct was cloned into a modified pFastBac1 vector (Invitrogen) containing an expression cassette with haemagglutinin signal sequence at the N terminus, and a PreScission protease site, 10 $\times$ His, and Flag tag at the C terminus. The BRIL-GCGR( $\Delta$ ECD/ $\Delta$ C) fusion construct was expressed in Sf9 cells using the Bac-to-Bac baculovirus expression system as described previously<sup>45</sup>. Sf9 cells at a density of  $2 \times 10^6$ – $3 \times 10^6$  cells ml<sup>-1</sup> were infected with P1 or P2 virus at a multiplicity of infection (m.o.i.) of 7.5. Cells were harvested less than 48 h post-infection and cell pellets were stored at  $-80^\circ\text{C}$  until used.

**BRIL-GCGR( $\Delta$ ECD/ $\Delta$ C) fusion construct purification.** Sf9 membranes were prepared with 1 wash cycle of hypotonic buffer (25 mM HEPES, pH 7.5, 10 mM MgCl<sub>2</sub>, 20 mM KCl) in the presence of EDTA-free protease inhibitor cocktail tablets (Roche) and 4 wash cycles of high-salt buffer (25 mM HEPES, pH 7.5, 1 M NaCl, 10 mM MgCl<sub>2</sub>, 20 mM KCl). Membrane pellets were homogenized in storage buffer (25 mM HEPES, pH 7.5, 500 mM NaCl, 40% glycerol), flash frozen in liquid nitrogen and stored at  $-80^\circ\text{C}$  until use.

The GCGR antagonist ligand NNC0640 (Supplementary Fig. 1b) was essential for purification and crystallization of the BRIL-GCGR( $\Delta$ ECD/ $\Delta$ C) fusion construct. Two grams of washed membranes containing the BRIL-GCGR( $\Delta$ ECD/ $\Delta$ C) fusion construct were resuspended in 30 ml of buffer (25 mM HEPES, pH 7.0, 166 mM NaCl, 13.3% glycerol) and incubated with 270  $\mu\text{M}$  of compound NNC0640 for 30 min at room temperature. The receptor was solubilized with 1/0.1% (w/v) of *n*-dodecyl- $\beta$ -D-maltopyranoside (Anatrace) and cholesteryl hemisuccinate (Sigma) (DDM/CHS) for 2 h at  $4^\circ\text{C}$ . The insoluble material was pelleted by ultracentrifugation in a Ti70 rotor at 504,300g for 30 min at  $4^\circ\text{C}$ . The NaCl and DDM/CHS concentrations of the supernatant were adjusted to 800 mM and 0.5/0.05%, respectively, by adding equal volume of talon binding buffer (25 mM HEPES, pH 7.0, 1.475 M NaCl, 10% glycerol). Protein was bound to 2 ml of talon superflow resin slurry (Clontech) overnight at  $4^\circ\text{C}$  on a rotor in the presence of 15 mM imidazole, pH 7.5, and 100  $\mu\text{M}$  NNC0640.

The talon resin was washed with 10  $\times$  bed volume of wash buffer 1 (25 mM HEPES, pH 7.0, 800 mM NaCl, 10% glycerol, 0.04/0.008% DDM/CHS, 30  $\mu\text{M}$  NNC0640, 40 mM imidazole, pH 7.5). Detergent concentration was lowered by washing the resin with 20  $\times$  bed volume of wash buffer 2 (25 mM HEPES, pH 7.0, 500 mM NaCl, 10% glycerol, 0.02/0.004% DDM/CHS, 30  $\mu\text{M}$  NNC0640). The BRIL-GCGR( $\Delta$ ECD/ $\Delta$ C) fusion construct was eluted with 2.5 ml of elution buffer (25 mM HEPES, pH 7.0, 150 mM NaCl, 10% glycerol, 0.02/0.004% DDM/CHS, 30  $\mu\text{M}$  NNC0640, 300 mM imidazole, pH 7.5). The eluted BRIL-GCGR( $\Delta$ ECD/ $\Delta$ C) fusion construct was desalted with a PD-10 desalting column (GE Healthcare) to remove the imidazole. His-tagged PreScission protease was added to the samples and incubated overnight at  $4^\circ\text{C}$  to remove the C-terminal 10 $\times$ His and Flag tags. Reverse talon purification was performed to isolate the cleaved BRIL-GCGR( $\Delta$ ECD/ $\Delta$ C) fusion construct by flowing the sample through 200  $\mu\text{l}$  talon superflow resin twice. The flow-through material, containing the cleaved BRIL-GCGR( $\Delta$ ECD/ $\Delta$ C) fusion construct, was concentrated to 80 mg ml<sup>-1</sup> using a Vivaspin centrifuge concentrator (GE Healthcare) with a 100 kilodalton (kDa) molecular weight cut-off.

**BRIL-GCGR( $\Delta$ ECD/ $\Delta$ C) fusion construct lipidic cubic phase (LCP) crystallization.** For LCP crystallization, the BRIL-GCGR( $\Delta$ ECD/ $\Delta$ C) construct was mixed with molten lipid at a ratio of 40/60% (v/v) using a mechanical syringe mixer<sup>42</sup>. Due to the high detergent concentration, 10–15% (volume of LCP) of 5 M NaCl was added after the lipid and protein were mixed to convert a destabilized lipidic mesophase into LCP<sup>46</sup>. The host lipid for the LCP reconstitution was monoolein (Sigma) with 10% (w/w) of cholesterol (AvantiPolar Lipids). Crystallization trials were set up as previously described<sup>47</sup>. LCP-FRAP was used to identify initial crystallization conditions that led to GCGR crystals<sup>48</sup>. Crystals were obtained at  $20^\circ\text{C}$  in 100 mM MES, pH 6.0, 140–200 mM Na/K tartrate tetrahydrate, 9–17% (v/v) PEG 400, 0.35–0.55% (v/v) Jeffamine M-600, pH 7.0, 200  $\mu\text{M}$  NNC0640; grown to a final size of 50–100  $\mu\text{m}$  in the longest dimension in about 5 days (Supplementary Fig. 3); and harvested from the LCP matrix using 50  $\mu\text{m}$  MiTeGen micromounts and immediately flash frozen in liquid nitrogen. **Data collection and processing.** X-ray data were collected at the 23ID-D beamline (GM/CA CAT) at the Advanced Photon Source (Argonne, Illinois) using a 20- $\mu\text{m}$  minibeam at a wavelength of 1.0330 Å and a MarMosaic 300 charge-coupled device

(CCD) detector. Crystals were aligned and data collected using a strategy similar to other GPCR structures<sup>49</sup>. Typically, 10–15 frames at  $1^\circ$  oscillation and 1–2 s exposure with non-attenuated beam were collected per crystal due to the fast onset of radiation damage. A 93.9% complete at 3.3 Å data set was obtained by indexing, integrating, scaling and merging data sets from 14 crystals using HKL2000 (ref. 50). Analysis of the final data set by the UCLA diffraction anisotropy server (<http://services.mbi.ucla.edu/anisocscale/>) indicated that diffraction along the  $b^*$  axis was weaker than in the other two directions; therefore, reflections were subjected to a mild anisotropic truncation with resolution limits of 3.3, 3.4 and 3.3 Å along  $a^*$ ,  $b^*$  and  $c^*$ , respectively, before using them in the refinement.

**Experimental phasing.** Initial attempts to find a molecular replacement solution using previous class A GPCR structures as search models in Phaser<sup>51</sup> did not generate any reliable solutions. Therefore, experimental phasing for the BRIL-GCGR( $\Delta$ ECD/ $\Delta$ C) fusion construct was attempted by soaking the crystals with different heavy atoms. After screening many crystals, a SAD data set was obtained from one crystal that was soaked overnight with 100 mM tantalum bromide (Ta<sub>6</sub>Br<sub>12</sub>) cluster (Jena Bioscience). The data were collected on the 23ID-D beamline (GM/CA CAT) at the Advanced Photon Source using the peak wavelength from the tantalum L3 edge (9.880 keV). A beam size of 10  $\mu\text{m}$  with  $5\times$  attenuation with  $1^\circ$  oscillation and 1 s exposure per frame was used. A complete  $360^\circ$  data set was acquired from a single crystal by collecting wedges of  $30^\circ$  with direct and inverse beam and translating 6 times along the crystal length to expose a fresh portion of the crystal for each wedge. The SAD data set was integrated and scaled at 4 Å resolution using HKL2000. PHENIX.AutoSol<sup>52</sup> was used to search for the heavy atom sites with anomalous signals at 6 Å resolution (Supplementary Fig. 7), yielding initial electron density maps.

**Structure determination and refinement.** While the experimental phasing work was underway, ‘mixed model’ molecular replacement (MR) search templates were generated based on all known GPCR structures using PHENIX.ROSETTA<sup>53</sup>. The ‘mixed model’ templates were then superimposed together and manually trimmed to remove structurally poorly conserved regions. Parallel MR searches with Phaser were then carried out using these GPCR models along with the high resolution BRIL structure (PDB: 1M6T) as search models on a linux cluster<sup>54</sup>. The search template based on rhodopsin (PDB: 2Z73) produced a potential solution (TFZ = 8.5). This MR solution was validated by the experimental phasing maps (Supplementary Fig. 8), and by the appearance of density not present in the search model. The experimental SIRAS phases calculated from the heavy atom were good up to 6–7 Å. However, SIRAS phases did not improve the MR maps, and thus were not used in the final refinement.

All refinement was performed using the MR solution with rounds of REFMAC5 (ref. 55), autoBUSTER<sup>56</sup> (Buster v2.8.0), and PHENIX.AutoBuild<sup>57</sup>, followed by manual examination and rebuilding of refined coordinates in COOT<sup>58</sup> using both  $2|F_o| - |F_c|$  and  $|F_o| - |F_c|$  maps, as well as omit maps calculated using the Bhat procedure<sup>59</sup> (Supplementary Fig. 9). We state 3.4 Å as the overall effective resolution of this structure; however, data to 3.3 Å were included in refinement, which improved the  $R/R_{\text{free}}$  statistics (Supplementary Table 2).

At 3.4 Å resolution, the electron densities for the majority of residues in the GCGR 7TM structure are visible, except for residues Arg 201–Trp 215 (corresponding to ECL1), and therefore these residues were not built into the GCGR 7TM structure. Residues Gly 269–Met 276, Thr 296–Asp 299, Ile 315–Ile 317, and Phe 365–Glu 371 were built into the GCGR structure, but they contained breaks in the electron densities of the C $_{\alpha}$  backbone. Hence, other conformations are possible for these residues.

Although we do not observe density for NNC0640 in the canonical ligand binding pocket, this ligand is required to obtain diffraction quality crystals of the BRIL-GCGR( $\Delta$ ECD/ $\Delta$ C) construct. There are two electron density blobs outside of canonical ligand-binding pocket, one at the bottom of helix VI and VII near Lys 349<sup>6,40</sup>, and the other at helix I near Trp 145<sup>1,43</sup>. However, both of them are too small to accommodate NNC0640.

**Energy-based conformational modelling of the GCGR–glucagon complex.** Glucagon was docked into the crystal structure of the GCGR ECD (PDB: 4ERS, residues 28–123) (ref. 6) using the crystal structure of the closely related GLPIR–GLP1 complex (PDB: 3IOL)<sup>8</sup> as a template. All molecular modelling and docking was performed using ICM molecular modelling software<sup>60</sup> (v. 3.7). The initial  $\alpha$ -helical conformation of glucagon peptide residues 11–29 was modelled based on GLP1 residues 17–35, and soft tethers between corresponding backbone C $_{\alpha}$  atoms of glucagon and GLP1 were applied. Conformation of the glucagon peptide and the interacting side chains in the ECD binding pocket were optimized (3 independent simulations of  $10^6$  steps) using ICM global optimization procedure in internal coordinates<sup>60,61</sup> with improved conformational energy terms for protein and peptides<sup>4</sup> and ‘tether weight’ = 0.1.

The model of the ECD–glucagon complex was then docked and optimized with the crystal structure of the 7TM domain, completed with all side chains and ECL1.

This flexible energy-based docking/optimization procedure involved all torsion coordinates in the regions that are not defined by crystal structures, including protein backbone in the residues 1 to 10 of glucagon, and GCGR residues in ECL1 (199–218), and linker (122–126). In addition, side chain torsion variables were set free in all glucagon residues and the following regions of the GCGR model: helix I stalk region (125–136), ECL2 region (289–310), ECL3 (368–377), as well as 31 other residues lining the 7TM binding pocket.

The following three soft harmonic restraints derived from experimental crosslinking data in GLP1R and GLP1 (ref. 12) were applied between glucagon and GCGR side chains to guide docking: F6(cb)–Gln 142<sup>1.40</sup>(cd), Y10(cb)–Tyr 138<sup>1.36</sup>(oh), L14(cb)–Trp 295<sup>ECL2</sup>(ch2). Two intramolecular harmonic restraints were also applied to glucagon residues, T7(og1)–Y10(n) and F6(cz)–Y10(cz), to facilitate N-capped formation in glucagon, as suggested by previous comparative studies of class B peptide ligands<sup>33</sup>. Finally, a restraint was applied between the positively charged N-terminal amino group of glucagon and the carboxyl group of Glu 362<sup>6.53</sup>. The importance of the carboxyl group of Glu 362<sup>6.53</sup>, which is the only negatively charged residue in the 7TM binding pocket, is supported by GCGR (Supplementary Table 5) and GLP1R (ref. 29) mutation studies (Supplementary Table 6). As the N terminus is the only basic moiety in the first 10 residues of glucagon, a potential Glu 362<sup>6.53</sup> salt bridge with the glucagon N terminus is the most likely explanation for the mutation effects in Glu 362<sup>6.53</sup>. A total of 164 torsion variables were systematically sampled with ICM Monte-Carlo global optimization, and 455 were locally minimized in the course of this procedure. The special 'local' sampling option was applied to the ECL1 region backbone to allow efficient optimization. Three independent runs of the global optimization procedure (10<sup>7</sup> steps each) resulted in similar best energy conformations within 2.5 Å r.m.s.d. for the glucagon peptide non-hydrogen atoms.

It should be noted that in the absence of glucagon, the ECD is likely to be more flexible, sampling multiple orientations relative to the 7TM domain<sup>6</sup>. The model also does not attempt to infer a specific functional state of the receptor, partially because such a state is not precisely defined for the 7TM crystal structure itself. For instance, NNC0640 used to stabilize the 7TM receptor fragment is a competitive antagonist to glucagon, which may have an effect on the crystallized conformation, even though NNC0640 is absent in the final structure. The accuracy of the GCGR–glucagon model may also be limited by the weak electron density of ECL2 and the top of helix V (residues 289–310), and the assumption that glucagon binds GCGR in an N-capped conformation<sup>7,33</sup>.

**Construction of GCGR mutants and cell transfection.** The complementary DNA (cDNA) encoding the human GCGR was originally obtained from GeneCopoeia and cloned into the expression vector pcDNA3.1/V5-His-TOPO (Invitrogen) at the HindIII and EcoRI sites. The single and double mutants were constructed by PCR-based site directed mutagenesis. CHO-K1 cells were seeded onto 96-well poly-D-lysine treated cell culture plates (PerkinElmer) at a density of  $2.7 \times 10^4$  cells per well. After overnight culture, the cells were transiently transfected with wild-type or mutant GCGR DNA using Lipofectamine 2000 transfection reagent (Invitrogen).

**Whole-cell glucagon binding assay.** Cells were harvested 24 h after transfections, washed twice and incubated with blocking buffer (F12 supplemented with 33 mM HEPES, pH 7.4, and 0.1% bovine serum albumin (BSA)) for 2 h at 37 °C. For homogeneous binding, the cells were incubated in binding buffer with constant concentration of <sup>125</sup>I-glucagon (40 pM) and different concentrations of unlabelled glucagon (0.02 nM to 5 μM) at room temperature for 3 h. Cells were washed three times with ice-cold PBS and lysed by 50 μl lysis buffer (PBS supplemented with 20 mM Tris-HCl, 1% Triton X-100, pH 7.4). The plates were subsequently counted for radioactivity (counts per minute, CPM) in a scintillation counter (MicroBeta2 Plate Counter, PerkinElmer) using a scintillation cocktail (OptiPhase SuperMix, PerkinElmer). Specific binding was determined by subtracting non-specific binding observed in the presence of 5 μM unlabelled glucagon.

**Expression level quantification of constructed GCGR in cells by flow cytometry.** Approximately  $1 \times 10^5$  transfected CHO-K1 cells were blocked with PBS containing 5% BSA at room temperature for 15 min and then incubated with 1:100 diluted primary antibody (anti-GCGR, Epitomics) at room temperature for 1 h. The cells were then washed three times with PBS containing 1% BSA followed by a 1 h incubation with anti-rabbit Alexa-488-conjugated secondary antibody (1:300, Invitrogen) at 4 °C in the dark. After washes, the cells were resuspended in 200 μl of PBS containing 1% BSA for detection in a flow cytometer (Accuri C6, BD Biosciences) using laser excitation and emission wavelengths of 488 and 519 nm, respectively. For each measurement, approximately 20,000 cellular events

were collected and fluorescence intensity of positive expression cell population calculated.

**NNC0640 binding assay (cell membrane based binding).** NNC0640 binding was analysed using plasma membranes prepared from HEK293T cells transiently expressing GCGR constructs. Approximately  $1.2 \times 10^8$  transfected HEK293T cells were harvested, suspended in 10 ml ice-cold membrane binding buffer (25 mM Tris-HCl, 0.1% BSA and 1 mM EDTA, pH 7.4) and centrifuged for 5 min at 200g. The resulting pellet was resuspended in cold membrane binding buffer, pulled through a 25G × 1 inch needle four times and centrifuged for 5 min at 20,000g. The precipitate containing the plasma membranes was suspended in membrane binding buffer containing protease inhibitor (Sigma-Aldrich) and stored at –80 °C. Protein concentration was determined using a protein BCA assay kit (Pierce Biotechnology).

For homogeneous binding, cell membrane homogenates (20 μg protein per well) were incubated in membrane binding buffer with constant concentration of <sup>3</sup>H-NNC0640 (50 nM, labelled by PerkinElmer) and serial dilutions of unlabelled NNC0640 (1.26 nM to 100 μM) at room temperature for 5 h. Nonspecific binding was determined in the presence of 100 μM NNC0640. Following incubation, the samples were filtered rapidly in vacuum through glass fibre filter plates (Millipore). After soaking and rinsing 4 times with ice-cold binding buffer, the filters were dried and counted for radioactivity in a scintillation counter (PerkinElmer).

**Western blot.** Protein samples were prepared as above, separated by 10% SDS-PAGE and transferred to nitrocellulose membranes. After a 2 h incubation with blocking buffer, the membranes were incubated with 1:1,000 primary antibody (anti-V5, Sigma) overnight. The membranes were then washed three times with TBS-T buffer (0.05 M Tris, 0.15 M NaCl, 0.1% (v/v) Tween) followed by a 2 h incubation with anti-mouse horseradish peroxidase-conjugated secondary antibody (1:1,000, Cell Signaling Technology). The membranes were washed again and then detected with SuperSignal West Dura Substrate (ThermoScientific) according to the manufacturer's instructions. Each membrane was exposed to X-ray film for detecting the blots. Bands were quantified with Quantity One Software (Bio-Rad).

**Statistical analysis.** Results are presented as means ± s.e.m. Changes in specific radiolabelled ligands binding and cell surface expression of GCGR constructs were normalized to those measured with wild-type GCGR control (100%). IC<sub>50</sub> values in binding assay were determined by nonlinear regression analysis using the Prism 5 software (GraphPad Software).

45. Hanson, M. A. *et al.* Profiling of membrane protein variants in a baculovirus system by coupling cell-surface detection with small-scale parallel expression. *Protein Expr. Purif.* **56**, 85–92 (2007).
46. Misquitta, Y. & Caffrey, M. Detergents destabilize the cubic phase of monoolein: implications for membrane protein crystallization. *Biophys. J.* **85**, 3084–3096 (2003).
47. Cherezov, V., Peddi, A., Muthusubramaniam, L., Zheng, Y. F. & Caffrey, M. A robotic system for crystallizing membrane and soluble proteins in lipidic mesophases. *Acta Crystallogr. D* **60**, 1795–1807 (2004).
48. Xu, F., Liu, W., Hanson, M. A., Stevens, R. C. & Cherezov, V. Development of an automated high throughput LCP-FRAP assay to guide membrane protein crystallization in lipid mesophases. *Cryst. Growth Des.* **11**, 1193–1201 (2011).
49. Cherezov, V. *et al.* Rastering strategy for screening and centring of microcrystal samples of human membrane proteins with a sub-10 μm size X-ray synchrotron beam. *J. R. Soc. Interface* **6** (Suppl 5), S587–S597 (2009).
50. Otwinowski, Z. & Minor, W. Processing of X-ray diffraction data collected in oscillation mode. *Methods Enzymol.* **276**, 307–326 (1997).
51. McCoy, A. J. *et al.* Phaser crystallographic software. *J. Appl. Crystallogr.* **40**, 658–674 (2007).
52. Terwilliger, T. C. *et al.* Decision-making in structure solution using Bayesian estimates of map quality: the PHENIX AutoSol wizard. *Acta Crystallogr. D* **65**, 582–601 (2009).
53. Terwilliger, T. C. *et al.* phenix.mr\_rosetta: molecular replacement and model rebuilding with Phenix and Rosetta. *J. Struct. Funct. Genomics* **13**, 81–90 (2012).
54. Schwarzenbacher, R., Godzik, A. & Jaroszewski, L. The JCSG MR pipeline: optimized alignments, multiple models and parallel searches. *Acta Crystallogr. D* **64**, 133–140 (2008).
55. Murshudov, G. N., Vagin, A. A. & Dodson, E. J. Refinement of macromolecular structures by the maximum-likelihood method. *Acta Crystallogr. D* **53**, 240–255 (1997).
56. BUSTER v. 2.8.0 (Global Phasing, Cambridge, UK 2009).
57. Terwilliger, T. C. *et al.* Iterative model building, structure refinement and density modification with the PHENIX AutoBuild wizard. *Acta Crystallogr. D* **64**, 61–69 (2008).
58. Emsley, P., Lohkamp, B., Scott, W. G. & Cowtan, K. Features and development of Coot. *Acta Crystallogr. D* **66**, 486–501 (2010).
59. Bhat, T. Calculation of an OMIT map. *J. Appl. Crystallogr.* **21**, 279–281 (1988).
60. ICM Manual v. 3.0 (MolSoft, La Jolla, California 2012).
61. Arnaoutova, Y. A., Abagyan, R. A. & Totrov, M. Development of a new physics-based internal coordinate mechanics force field and its application to protein loop modeling. *Proteins* **79**, 477–498 (2011).